Engineering Failure Analysis 146 (2023) 107058

Contents lists available at ScienceDirect

Engineering Failure Analysis

journal homepage: www.elsevier.com/locate/engfailanal

An experimental and numerical study of the solid particle erosion damage in an industrial cement large-sized fan

Annalisa Fortini *, Alessio Suman, Nicola Zanini

Department of Engineering – University of Ferrara, Ferrara, Italy

ARTICLE INFO

Keywords:
Wear damage
Hardfacing
Centrifugal fan
Computational fluid dynamics
Solid particle erosion
Metallographic analysis

ABSTRACT

The present paper addresses the wear failure analysis of a large-sized centrifugal fan operating in a cement clinker grinding plant. Within cement production, the calcination at middle and high-temperature values (from 120 °C to 400 °C depending on the process parameters) of the raw material requires such a process fan, which also ensures the draft and feed of the flue gases and combustion air needed for the operation of the main equipment of the cement factory. To detect and analyze the impact conditions within the heavy-duty fan, Computational Fluid Dynamics (CFD) analyses were performed. The analysis of the numerical results shows that the relevant fan surfaces are affected by different impact velocities and angles, generating non-uniform erosion patterns similar to the on-field detections. Besides, the obtained comprehensive description of the flow and contaminants behaviors through the entire flow path enables setting up the subsequent experimental investigation. The erosive wear behavior of a Fe-Cr-C hardfacing cast iron and wear-resistant steel was tested through a test rig constructed for the purpose of being in accordance with the ASTM G76 standard. The test bench was adapted to manage the raw meal powder used in the cement factory to reproduce the actual operating conditions. The results show a greater capability of Fe-Cr-C hardfacing cast iron to face the erosion phenomenon in terms of lower values of material loss over the exposure time. These findings, coupled with the metallographic analysis to detect the erosion mechanisms (ductile and/or brittle), help a better prediction of the fan operating life. The investigation showed the reliability of the numerical/experimental coupled approach in assessing the actual erosion magnitude and the influence of the impact angle on the erosion phenomena. This coupled approach gains a further understanding of the proper design of manufacturing and maintenance activities, covering several project steps from material selections to the scheduled and overhaul operations. A reliable operating-life prediction allows manufacturers and operators to obtain production and economic goals.

1. Introduction

The progressive alteration or removal of material from the surface of components employed in machine parts and implants affects their performance, reliability, and service life and is responsible for the increased cost of maintenance, downtime, and safety risks.

Among the different wear processes, surface material loss due to erosive wear is a critical practical issue in the design and operation of machines working with fluid. The erosion process is typified by the mechanical interaction between impinging solid or liquid

* Corresponding author.
E-mail addresses: annalisa.fortini@unife.it (A. Fortini), alessio.suman@unife.it (A. Suman), nicola.zanini@unife.it (N. Zanini).

https://doi.org/10.1016/j.engfailanal.2023.107058
Received 10 November 2022; Received in revised form 31 December 2022; Accepted 10 January 2023
Available online 13 January 2023

particles carried by a multicomponent fluid and the surface [1]. More specifically, when material loss from a solid surface is due to repeated impacts from gas-borne solid particles, the so-called Solid Particle Erosion (SPE) takes place [1–3]. As a result of the mechanical interaction, the particles indent or fracture the surface, and the material is progressively worn away. The SPE notably affects machine components operating in dusty environments, as it happens for aero-engine compressor/turbine blades, aircraft propeller, wing leading edges, and rocket engine tail nozzles, and it is an ongoing widely investigated topic to limit and prevent failures [4–8].

Even if many investigations have been devoted to the erosion process, a comprehensive understanding of this phenomenon has not yet been reached, and this issue is highly topical [9]. In addition, it is even more complicated when thermal, chemical, or physical reactions occur on the surface exposed to erosion [3]. The SPE is a multi-driven phenomenon in which different mechanisms and parameters play a significant role, operating simultaneously and affecting each other throughout the process. Data from several studies claimed that the overall erosive wear resistance depends on the material-related particle features (i.e., chemical composition, size [10,11], shape [12], hardness [13,14,18], fracture toughness [19], yield stress, roughness, etc.) and the fluid mechanics' related particle properties (i.e., impact velocity [15,16], impact angle [17], number of restrikes [2], temperature [20,21], etc.). The severity of the damage is usually computed in terms of erosion rate (ER) that can be expressed as a mass loss of the removed material for the unit of mass of erodent or, in practical applications, as the mass of material removed for the unit of surface in the unit of time for a given erodent. As for the particles' features that affect the erosive behavior, the impact angle has a crucial role in the SPE, and there is a solid and consistent association between impact angle and material behavior. A widely accepted distinction concerns the type of erosion mechanisms: brittle materials show the highest ER with a normal angle (erosion increases monotonically with the impact angle), whereas ductile materials show the highest ER with angles less than 30° (erosion increases with impact angle up to 15° – 30° of impact angle, approximately between 15° – 30°, depending on the properties of the material, commonly). Besides, the shape of the particles is crucial since spherical-shaped particles do not remove materials, but they tend to only cold-work the surface, resulting in peenging deformation and residual compressive stresses [1]. In addition, an increasing trend of ER with impact velocity has been demonstrated and widely experimentally investigated considering different media [22,23].

Against this background and considering that the SPE is technically unavoidable, erosive wear is dealt with by wear-resistant alloys or protective treatments and coatings [24]. In some specific circumstances (i.e. mining industry, demolition equipment, waste recycling, iron and steel plants, cement works, asphalt or glass industries), machine components have to withstand severe loading conditions, and, within these highly demanding environments, they are continuously exposed to the harshest wear attacks. The weld deposition of a material with a greater hardness with respect to the substrate, typically low-carbon steel, is a technique widely used in many industrial circumstances in which resistance to wear, corrosive environment, and high temperature are required [25–28]. To extend the service life of critical components and to avoid costly machine downtime, ensuring a rewarding margin for the manufacturer, surface coatings are often applied only in correspondence with the part of the component most subject to wear attack. The obtained weld deposit, made by multiple layers and up to 10 mm thick, has excellent resistance to wear. Hardfacing may be applied to a new part during its production, or it may be used to restore a worn-down surface. This solution has an immediate economic advantage on the new component and an economic benefit that develops parallel to the life of the component by virtue of the reduction in repair/replacement costs of the damaged area only [29]. A large variety of hardfacing alloys can be welded on-site for protection against wear, and the selection of abrasion-resistant alloys acting as hardfacing layers is crucial. Depending on the application, different compositions of the hardfacing alloys can be employed: (i) the low-alloy iron-base materials, containing up to 12 % alloying elements, usually chromium, molybdenum, and manganese; (ii) the high-alloy iron-base materials, with 12 % to 50 % alloy elements (in addition to the chromium these alloys may also contain nickel or cobalt); (iii) the cobalt-base and nickel-base alloys, with relatively small amounts of iron (1.3 % to 12.5 %), of these, the most costly, but also the most versatile, are the cobalt-chromium-tungsten alloys; (iv) the tungsten carbide alloys, for which the most used base material is steel, and, depending on the specific application, the content of carbon can change.

Among the commercially available materials for abrasive wear applications [3], High Chromium Cast Irons (HCCIs) are frequently used, given their superior erosion resistance in conjunction with the economic benefit which arises from their availability as welding consumables. The iron-chromium alloys usually employed in mining, digging, wrecking, and drilling machines are based on white iron foundry technology [1]. The ASTM A532 standard refers to abrasion-resistant cast irons used for mining, milling, earth handling, and manufacturing industries that have been engineered to offer high abrasion resistance [30]. According to the Fe-Cr-C phase diagram, hyper-eutectic alloys comprise primary M_7C_3 carbides surrounded by a matrix of eutectic carbides and austenite. The addition of chromium greater than 12 wt. % forms the so-called HCCI: the chromium content leads to improved corrosion resistance but also promotes the formation of coarse hexagonal M_7C_3 carbides on solidification that are responsible for wear resistance. The excellent abrasive and erosive wear resistance of such alloys depends on the high volume fraction of hard carbides that act as effective barriers to chipping and plowing by erodent particles. In addition to the M_7C_3 carbides, other types of carbides could be present in relation to the carbon and chromium contents. In this respect, to design alloys with both good mechanical properties and high wear resistance, strong carbide-forming addition is a well-known approach. Specifically, molybdenum increases hardenability and also creates abrasion-resistant particles, i.e. Mo-rich carbides.

It has been established that the wear response of a specific system depends on the tribological conditions, and several laboratory tests have been developed to simulate the acting wear mechanisms, even if for the determination of the realistic tribological behavior, field tests should be carried out [31]. Laboratory-scale erosion tests are usually performed for three main reasons: to provide data on absolute and relative wear rates under specific conditions, to validate predictive models, and to study the wear mechanisms [32,33]. It is worth noting that the operating conditions, i.e., particle velocity, erodent particle type and size, and impact angle, are crucial and must be accurately defined so that such tests' results are reproducible and valuable in practical applications [32]. Among the several test methods, the ASTM G76 test standard [34] is intended for testing erosion behavior through 50 μm aluminum oxide as

impingement particles: they are accelerated in a gas stream and hit the surface of the material to be tested with an impact velocity capable of penetrating most of the coatings and severely damaging all the materials. Despite that, much of the available literature on the erosive wear process on hardfacing alloys deals with laboratory tests such as the dry sand-rubber wheel [35–40] (according to the ASTM G65 standard), and only a few studies have addressed the SPE phenomena through on-purpose gas-blast test rigs [41–44].

1.1. Heavy-duty fan-related issues

As part of mining and mineral processing, severe mechanical interactions between metals and abrasive metallic and nonmetallic media occur and cause considerable wear damage to handling and processing equipment [3]. Within the raw mineral processing, comminution and sizing operations involve the handling of coarse and fine particles from different minerals, which, together with the combined effects of high impact, compression load, and sliding of abrasive feed, results in severe wear attack phenomena. Heavy-duty centrifugal fans are employed in process industries for cement, steel, and energy production. In these areas, exhausters are used for different purposes: e.g., in the metallurgical field, they are employed for agglomeration, where dust from the agglomeration process passes through them, and in heating and power plants, where ash particles are suspended in the airflow. Heavy-duty fans are energy-consuming machines: in cement manufacture, they can consume up to 30 % of the total electrical power used in the whole plant [45]. Where these fans are employed in industrial processes that also involve the operation of contaminated gases, they have to withstand high dust loads or wearing media and simultaneously offer high efficiency and reliability. Wear resulting from abrasion mechanisms can severely jeopardize the performance of the turbomachine (i.e., erosion issues, unbalanced loads, vibrations, structural damages) and, at worst, promote early and unforeseen failures. The resulting economic losses can be very severe [46], especially if these occurrences generate unpredictable plant stops.

The production of clinker, the base material of the Portland cement, is a typical example of a process where the calcination at a high temperature of the raw material, pulverized by mills and crushers, is delivered by centrifugal fans placed in the most critical points of the plant. The cement manufacturing process begins with mining and grinding raw materials, which include limestone and clay, to a fine powder called raw meal, which is then heated to a sintering temperature at about 1450 °C in a cement kiln to obtain the clinker. Industrial fans are used in cement production and comprise forced draft fans, involved in many phases of the process, and induced draft fans, employed in the exhaust fumes treatment to generate a negative pressure airflow to guarantee the proper work of the dust abatement system in the filtration device. Throughout the cement production process, fans are exposed to extreme demands related to high temperatures, up to 400 °C, and abrasive media dragged by gasses, whose velocities can reach up to 100 m s^{-1} in the internal passage of the machine. The abrasive particles carried by the airflow damage the overall materials of the systems. The particles strike the surfaces (i.e., the blades, shroud, and backplate of the impeller and the casing) following a force balance between drag and lift forces, leading to a material removal process related to the impact conditions, which are different through the machine flow path.

The role of centrifugal fans within cement factories was pointed out by McKervey and Perry [47], who highlighted that the most beneficial improvements to kiln systems come from modifications or replacements of fans. The authors also reported some case histories of fan erosion problems during operation. In 1980, the research laboratories of the Westinghouse Electric Corporation of Pittsburg (Pennsylvania) surveyed power plants having units larger than 100 MW generating capacity and using pulverized coal-fired boilers. The results of this survey are reported in a technical report from Glasser et al. [48], whose findings showed that erosion damage is mainly located on blade leading edges, trailing edges, and fan center plates. The erosion of the leading edges was the most severe one. The authors also highlighted that: (i) 71 % of gas-recirculating fans required erosion-caused repairs, and 22 % of these experienced moderate to heavy erosion damage; (ii) 39 % of the induced draft fans required erosion-caused repairs, and 14 % of these experienced moderate to heavy erosion damage; (iii) 68 % of scrubber booster fans experienced no erosion damage, 26 % experienced slight erosion, and 6 % no erosion at all; (iv) just 1 % of primary air fans experienced high erosion; and (v) forced air fan erosion was minimal (98 % of them had no erosion issues). They estimated that a total of 27,000 man-hours was being used annually to repair erosion damages in these machines and that the cost of purchasing replacement power during overhaul operation was around 11 million dollars per year.

The severe erosive conditions under which these machines operate determine a progressive reduction in the wall thickness of specific fan zones, which may finally result in the formation of holes. As stated above, erosion-resistant overlays are frequently used in such large components to prevent and/or limit erosive damage. Wear-resistant plates, made up of an hardfacing alloy layer weld-deposited on a base plate, are usually located in correspondence to the fan zones more affected by particle impacts. The benefits of this solution are reported by Mandi and Yaragatti [49]. Besides these methods to improve wear resistance, a forward-thinking approach consists of the prediction of wear occurring in industrial applications through Computational Fluid Dynamics (CFD) models, able to investigate the effects of micro-sized particle impact [50,51] and the effects of the erosion damage on the performance of the fan and the production system [52], as well as the occurred failure mechanisms [53,54].

Hence, together with fault detection, the fan may also be the subject of a flow simulation, customized to its operation, to determine how the fan may best be protected against wear. Through CFD, the establishment of optimal wear protection, in terms of its positioning and design, could be effectively predicted. Considering the specific properties of the abrasive material, the load on the blade's leading edge could be numerically computed, and this would be technically impossible or disproportionately costly to capture using measurement technology. As for specific studies that have described the erosion of centrifugal fans, Menguturk and Sverdrup [55] carried out numerical simulations on fly-ash particle trajectories considering the ER for four different types of centrifugal fans to compare their resistance to erosion phenomena. The authors reported that airfoil centrifugal fans show the highest fly-ash erosion tolerance, although their sensitivity to fan unbalance due to partial filling of blades with ash restricts their use for duty in erosive situations. Concerning this aspect, such an investigation highlighted that the use of single-thickness, backward-curved blading in a wide airfoil fan wheel

would overcome the sensitivity of this fan type to unbalance problems with a minor efficiency penalty. In a recent study by Cardillo et al. [56], unsteady numerical simulations were employed to analyze the erosion of the impeller of a large centrifugal fan installed in a cement production plant. The authors modeled contaminant (5 μm particles) transport and turbulent dispersion using a Lagrangian approach coupled with a particle cloud tracking model. The analysis highlighted non-uniform erosion patterns due to the large unsteadiness and the inherent distortion of the impeller flow as per the impeller-volute interaction. More recently, Fritsche et al. [57] analyzed the erosion behavior of large radial fans in recycling plants for end-to-life vehicles. They explored the respective influence of the spiral volute and blade shape on the erosion rate employing CFD simulations. It was demonstrated that, for the typical parameters of the investigated fans, the impact angle of metal contaminant (1 mm particles) has a stronger influence than the particle impact velocity. Larger volute designs (i.e. larger spiral pitch angles for volute) were found preferable from an erosion point of view, not because the velocity at their walls is substantially low, but because the particles have steeper angles of incidence and hence cause smaller erosion damage at the walls. In addition, they showed that smaller blade exit angles (i.e. impellers with backward curved blades) determine fewer erosion rates on the blades as well as on the volute wall.

1.2. Aim of the paper

In light of the challenges concerning erosive damage and material improvements to face wear degradation, this case study seeks to examine the failure that occurred on a large-sized centrifugal fan employed in a clinker production plant, tackling the erosion issues by twofold sides using numerical and experimental tools. The erosion issue in a heavy-duty industrial fan is a complex phenomenon strongly related to the interaction between the fluid phase, solid particles, and stationary and rotating fan components. The investigation of the phenomenon is crucial to increase the knowledge and set up an effective countermeasure to improve the reliability of the entire system and reduce the maintenance time and costs with a greater capacity utilization rate of the plant. With all these considerations, the present work reports numerical and experimental investigations performed to address the occurred failure. The role of the material in the enhancement of the service life of components (allowing a more precise prediction of service intervals) was evaluated after a precise characterization of the actual installations. The numerical investigation leads with the characterization of the flow inside the heavy-duty fan to study the flow and contaminants behaviors through the entire flow path and to detect the impact conditions (in terms of velocity and angle values) and the impact regions. This analysis has twofold aims: the first one is the setup on the impact characteristics to have a reference for the subsequent experimental investigation, and the second one is the validation of the numerical model in terms of eroded regions to consider the future fan improvements employing a computation analysis before the actual installation (the size of the fan does not lend to the creation of prototype). The experimental investigation compares the wear resistance of a Fe-Cr-C hardfacing cast iron and wear-resistant steel. The erosive wear damage was tested through a test rig constructed for the purpose of being in accordance with the ASTM G76 standard but pointed towards the employment test of the raw meal powder commonly used in a cement factory. The impact conditions are computed from the numerical analysis to focus the experimental investigation only on the involved operating condition, ensuring that the characterization of the former materials and the hypothesized substitutive materials will effectively reduce the erosion issues of the machine, thus increasing fan operability.

2. Overview of the failure

2.1. Failure description: process

The fan investigated in the present study is a large-sized single-inlet centrifugal fan that had been in service for three years in a cement plant, the Aalborg Portland cement plant (Denmark). The latter is the only grey, and white cement producer in Denmark with an annual capacity of approximately 3 million tons, of which 2.1 million are grey cement and 0.9 million are white cement. The peculiarity of this production plant is the operating temperature. The application refers to humid cement production, with a maximum

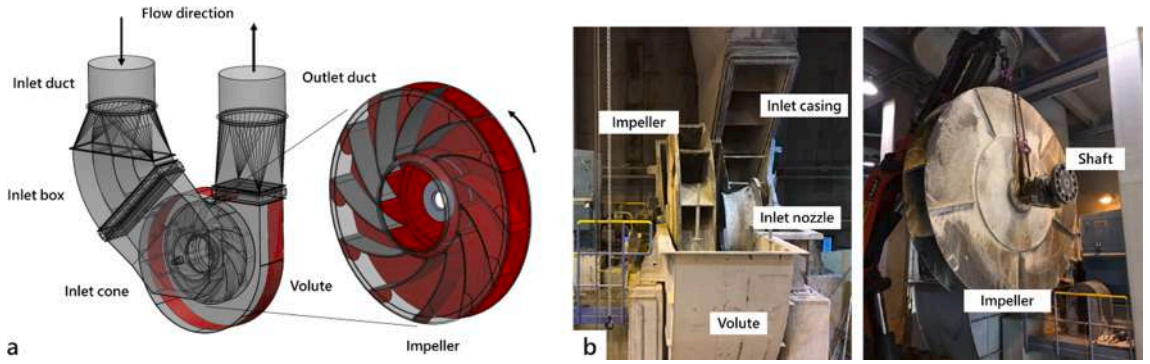

Fig. 1. (a) three-dimensional drawing of the centrifugal fan with the location of the wear-resistant plate labeled in red, (b) digital images of the in-service heavy-duty centrifugal fan within the cement production plant. (For interpretation of the references to colour in this figure legend, the reader is referred to the web version of this article.)

fan operating temperature of 120 °C.

The fan is composed of a vaned inlet airbox that deflects the flow from the radial inlet duct into the axial inlet cone. The fan impeller diameter is 4 m and is equipped with 12 backward-curved cylindrical blades. The impeller outflow was collected by a constant-width spiral volute. The transition from the inlet box to the impeller fan is managed by an inlet cone bolted to the front side plate of the volute. The heavy-duty process imposes a constant rotational velocity of the fan equal to 652 rpm, and it is characterized by a gas temperature of 120 °C with a 6.03 kg s^{-1} of raw meal powder (it corresponds to a contaminant concentration of 39 g m^{-3}). More details can be found in [50,51,58].

A typical on-field operation is to deposit wear-resistant plates (a layer of Fe-Cr-C hardfacing alloy on a low-carbon steel base plate) to mitigate erosion damage due to solid particle erosion of specific areas of the fan by the flux-cored arc welding method. Usually, wear-resistant plates are installed only on the more relevant fan regions, such as on the pressure side and at the leading edge of the blades, and a band of the spiral volute facing the impeller outlet section. Fig. 1 depicts the three-dimensional drawing of the considered centrifugal fan with the location of the wear-resistant plate labeled in red (Fig. 1a) and digital images of the in-service heavy-duty centrifugal fan within the cement production plant (Fig. 1b).

2.2. Visual inspection during overhaul

A visual inspection of several areas of the fan was performed to analyze the fan structure after 24,000 operating hours (almost three years) to detect the amount of damage and the fan regions involved in the erosion process. A detailed visual analysis of the unit is described as follows with reference to the images reported in Figs. 2 and 3.

Firstly, the analysis was devoted to detecting the erosion magnitude in the regions where hardfacing plates have been placed, i.e., covered zones. As can be seen in Fig. 2a,b severe erosive wear is localized on the leading edges of the blades, labeled with the red circle and the red arrows, respectively. The mass loss due to the mechanical action of the powder in the airflow impinging and abrading the surfaces is detectable from the visual examination and mainly affects the disk side of the impeller. Besides, erosion damaged some areas of the volute despite the presence of the hardfacing plates (Fig. 2c), promoting the formation of oriented grooves (see Fig. 2d, close-up of the circled region depicted in Fig. 2c) probably due to the combination of the drag forces provided by the airflow and contaminant inertia (see " Flow simulation findings: model validation" section for more details). Looking at these fan regions, it can be concluded that the hardfacing plates have protected the base material of the fan adequately. At the same time, localized regions (such as the blade leading edge) that play a crucial role in the fan performance appear affected by severe erosion damage showing a quiet delay in the overhaul operation.

Besides the protected regions, the overhaul operation has revealed other eroded fan regions. Looking at the stationary part of the fan, such as the volute and inlet cone, the inspection showed the presence of several damaged regions. Fig. 3a shows severe damage on

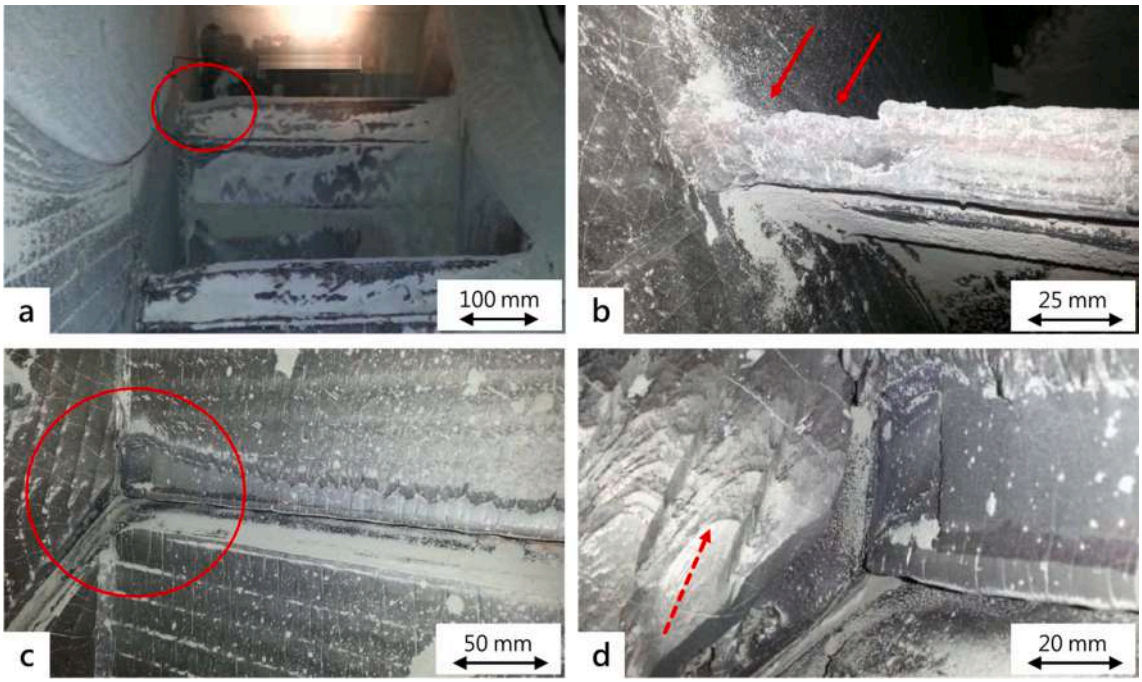

Fig. 2. Digital images of eroded fan regions, covered zones: (a), (b) severe erosive wear is localized on the leading edges of the blades, labeled with the red circle and the red arrows, (c) erosion damage on some areas of the volute and (d) close-up of the circled region depicted in (c). (For interpretation of the references to colour in this figure legend, the reader is referred to the web version of this article.)

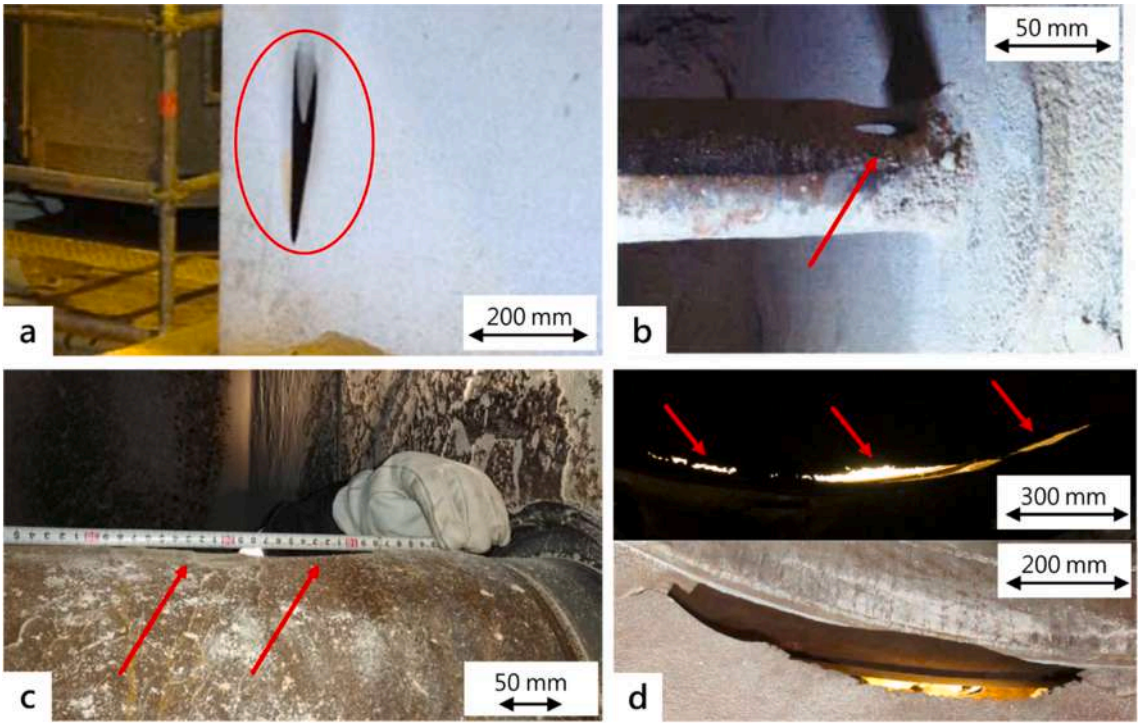

Fig. 3. Digital images of eroded fan regions, not covered zones: (a) localized erosion phenomena on the volute surface, (b) reinforced bars at the inlet duct, (c) erosive wear on the impeller shaft, (d) elliptical hole detected on the inlet cone surface and the cone boundary.

the volute surface, affected by a 200 mm-large hole, as the result of the localized erosion phenomena that occurred. Fig. 3b reports the damage at the reinforced bar at the fan inlet, positions to increase the structural strength of the inlet duct (see Fig. 1a). Fig. 3c illustrates a digital image of the failed fan with specific reference to the impeller shaft: the erosive wear due to the SPE had noteworthy reduced its thickness in correspondence to its center. Finally, the inlet cone inspection (see Fig. 3d) reports an elliptical hole (characterized by a major axis equal to 0.66 m and a minor axis of 0.13 m) which determines a disturbed flow field at the fan inlet (this condition could lead to a reduction of the hydraulic efficiency of the fan). In addition, this damaged condition determines the hydraulic connection between the entry flow (low-pressure fluid) and the recirculating flow in the volute (high-pressure fluid), generating a fan performance drop in terms of volumetric efficiency.

Due to operating conditions, powder characteristics, and installation, the assessment of the erosion behavior of the fan is focused only during the scheduled machine overhaul, when all the internal surfaces are checked and subjected to an accurate inspection. For these reasons, numerical and experimental approaches have to be used to study and interpret the on-field evidence to increase the

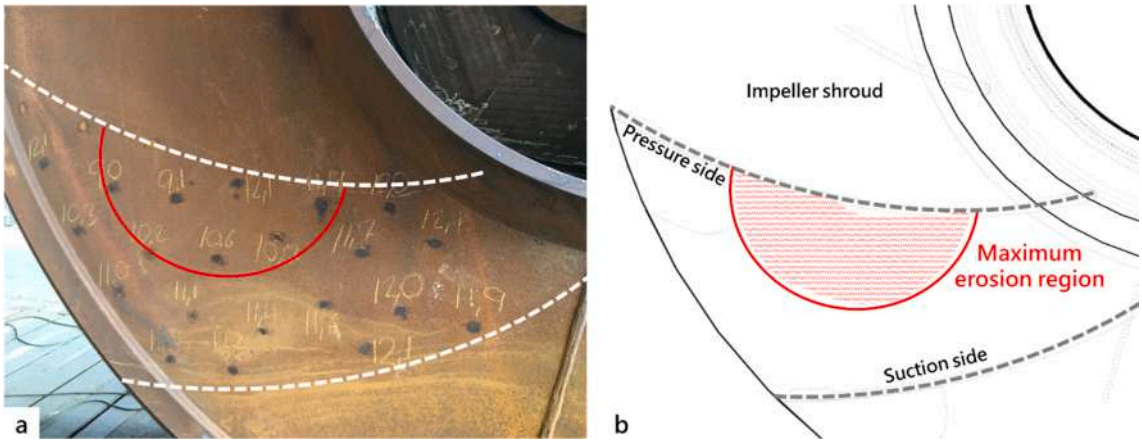

Fig. 4. Ultrasonic thickness measurement: (a) digital image of the impeller with the thickness data [mm] and the superimposition of the blade profile and the maximum erosion region, (b) sketch of the investigated region in (a).

knowledge and set up design improvements to increase the prediction of the erosive effects.

2.3. Residual thickness evaluation

In conjunction with the visual inspection, a quantitative evaluation of the erosion damage has been carried out. As stated above, erosive wear damage is responsible for the reduction of the service life of the fan, whose associated costs are noteworthy. In analyzing the effects of the wear phenomenon, a key factor is to measure the thickness of the remaining material. One of the practical material thickness evaluations through a non-destructive approach is through an ultrasonic device. This helps the identification of the most-affected area but, at the same time, gives a chance to collect data for predicting the remaining service life of the components. The detection of the material loss is thus pivotal for localizing the maximum erosion regions and assessing the periodical maintenance of the components. Furthermore, despite the absence of macroscopic erosion-related effects (such as holes and cracks) on the rotating parts, the material loss could generate unbalanced loads responsible for vibration and structural damage.

Fig. 4a displays a digital image of the on-site evaluation of the material thickness measured by an ultrasonic thickness gauge (Elcometer PTG8, Elcometer, Manchester, UK). Data in Fig. 4a show that the thicknesses range from 13.1 mm to 9.0 mm, indicating the critical areas that have experienced significant material loss due to erosion. It is worth noting that the nominal thickness is 15 mm. As can be seen, the erosion of the impeller is localized in the impeller channels, as labeled by the red line and in the corresponding sketch of Fig. 4b.

2.4. Numerical modeling

A CFD analysis of the entire unit has been done to investigate and quantify the magnitude of the relevant characteristics of the contaminant impact on the fan surface. The unit was modeled from the inlet duct section to the outlet discharge section to account for the interaction between the contaminated airflow and the stationary and rotating parts. As stated above, the erosion issue was driven by the impact of micro-sized solid particles on the fan surface. The former step to this end is a reliable prediction of the trajectories of the particles. A multiphase strategy based on a resolution of the continuous media by the Eulerian approach and resolution of the discrete phase by the Lagrangian approach has been done.

The complete assessment of the numerical model can be found in [50,51]. For the sake of completeness, a brief description of the main numerical model features is reported in this work. The numerical investigation was carried out at the nominal mass flow rate (122 kg s^{-1}) corresponding to a total pressure of 8,300 Pa with an inlet temperature of 118 °C. Since the unit is used to supply the gas to

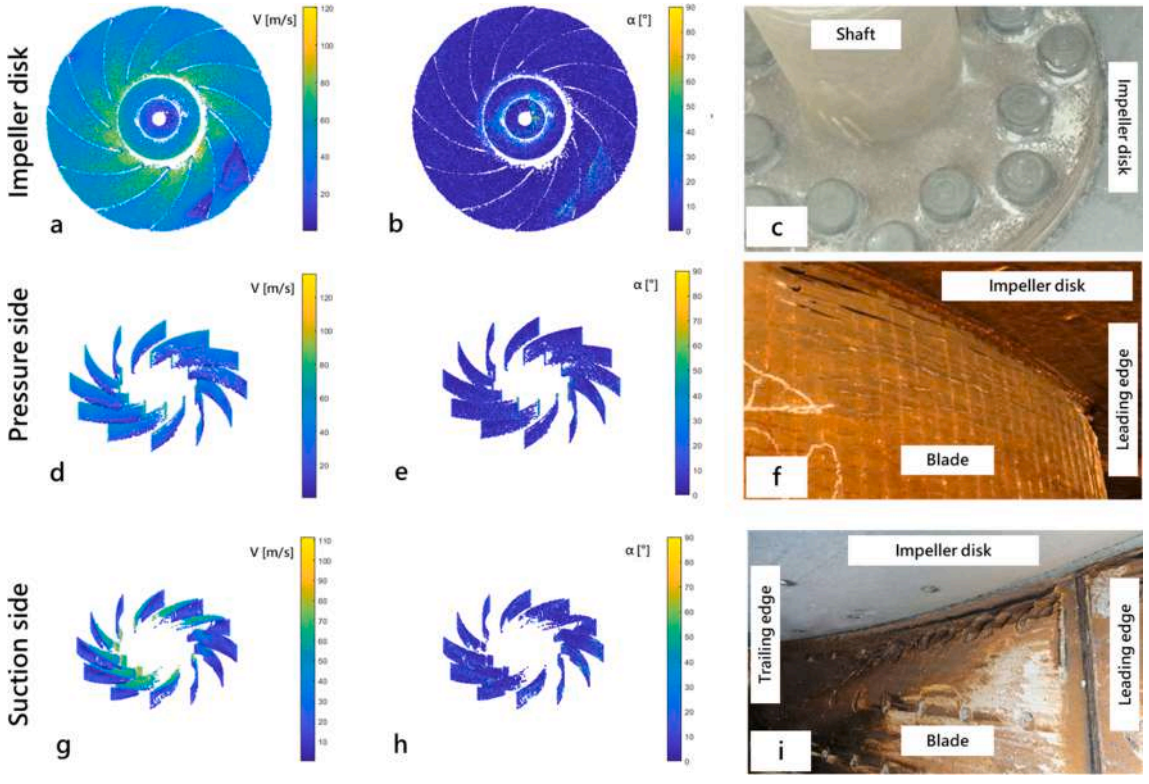

Fig. 5. Comparison between numerical predictions and on-filed detections on the rotating parts: (a), (d), (g) impact pattern in terms of velocity; (b), (e), (h) impact pattern in terms of angle; (c), (f), (i) digital images of the actual detections.

the furnace, the unit operates with an inlet gauge static pressure of −7,355 Pa. The kiln exhaust gas handled by the fan is approximated as an ideal gas with constant properties (specific heat, dynamic viscosity, and thermal conductivity). To solve the interaction between the impeller and the asymmetric volute, reducing the computational effort, the steady simulation of the fan operating point is performed at three relative positions between the impeller and volute. These relative positions are chosen within a single impeller pitch (equal to 30°), one each 10°rotation, and correspond to the passage of one impeller blade in front of the volute tongue. Overall fan performance is calculated by averaging the values from the three calculations. The steady calculation was assessed with reference to the unsteady analysis reported in [50].

According to the sketch in Fig. 1, the computational domain comprises the stationary parts generating a fully-three-dimensional domain meshed with about 57 million elements. To couple the accuracy of calculation to the computational effort, tetrahedral elements were used to discretize the internal volume, while prism layers were used in correspondence with the walls. The approach used to solve the stator rotor interaction and the computational grid allow the reduction of the computational effort giving a chance to use a comprehensive modelization of the discrete phase.

The discrete phase was modeled using a Lagrangian approach. Therefore, the airflow field is first simulated, and then the trajectories of individual particles are tracked by integrating a force balance equation on the particle, including also the contribution of the Saffman lift force due to the micro-sized dimension of the contaminants (see next paragraph for more details about the contaminant). To account for the turbulent dispersion, the Gosman and Ioannides model was added to the particle tracking strategy [59]. According to the production plant data (the contaminant concentration is equal to 39 g m^{-3}), it is assumed that particles do not affect the fluid flow (one-way coupling) as the particle's volume fraction is meager (≪ 10 %). Therefore, particles are released at the same local velocities as the gas flow from the inflow boundary of the inlet duct, with equally spaced randomly positioned injection points. The number of tracked particles is 10^6 to satisfy the statistical independence of the results since turbulent dispersion is modeled based on a stochastic approach. More details can be found in [50].

To validate the numerical model and, in turn, use reliable numerical results about particle impact for setting up the experimental campaign, a comparison between the on-field detection and the numerical impact patterns was conducted. As known, the erosion models, commonly used in numerical computation analysis [9], have to be fed by a set of coefficients representative of the materials in contact (substrate and particles) to consider the prediction reliable. For these reasons, the numerical campaign was set up to predict the impact velocity and angle to allow the definition of the closest dynamic impact parameter, leaving the prediction of the erosion issue to the experimental tests and data post-process.

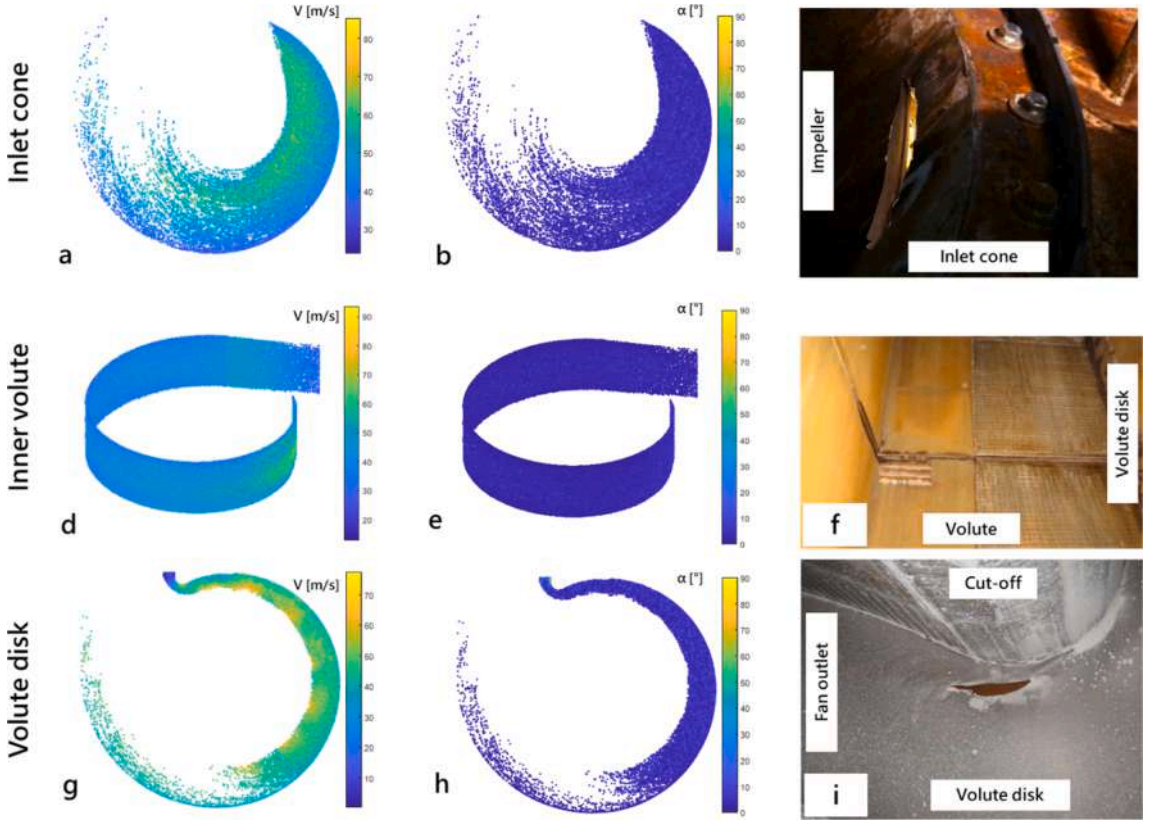

Fig. 6. Comparison between numerical predictions and on-field detections on the stationary parts: (a), (d), (g) impact pattern in terms of velocity; (b), (e), (h) impact pattern in terms of angle; (c), (f), (i) digital images of the actual detections.

Figs. 5 and 6 report the comparison between the impact pattern (in terms of velocity and angle) and the actual detections for the rotating and stationary parts, respectively. A preliminary assessment of the impact patterns has to be done, looking at the impact velocity and impact angle maps. According with the literature [22], higher velocity leads to more severe erosion. Regarding the impact angle, the definition of general rules is not trivial depending on the substrate behavior (ductile or brittle). At this step of the analysis, since the substrate material is an hardfacing alloy on a low-carbon steel base plate, it could be assumed that its erosion behavior is similar to ductile material and thus, moving from the normal impact to a tangential impact, the erosion phenomenon increases.

Fig. 5a b report the numerical results for the impeller disk and shaft. As can be seen from the pictures, the impacts are more detrimental in correspondence to the impeller disk center (shaft), where the impact velocity values are higher (Fig. 5a) and the impact angle values are lower (Fig. 5b). In this impeller region, there are several bolts and discontinuities due to the mechanical joints between the impeller and the shaft, which determine higher values for the impact angles (see Fig. 2a). Moving to the impeller blade, the most affected region is the leading edge. Looking at Fig. 5d, e, this region is affected by the highest values of velocity and the lowest values of impact angle that imposed the maximum erosion effects (leading edge erosion is also visible in Fig. 2a). The pressure and suction sides are interested in tangential impact angles, even if the flow separation in the suction side determines higher values of impact angles, especially close to the impeller disk (Fig. 5h). Looking at the detection (Fig. 5f, i), the traces of the particle impacts are evident, as predicted by the numerical results, where two different values of impact velocity can be noticed as a band, according to the blade span.

The last part of the numerical model validation is devoted to comparing the impact on the stationary part and the on-field detections (Fig. 6). Fig. 6a, b depict the impact, and Fig. 6c shows the failure that occurred to the inlet cone. From the numerical simulation results, it can be seen that the impacts are localized in a specific region of the cone in the proximity of the hole detection during the overhaul operation (Fig. 6a, b). On-field observations revealed that the damage is due to an erosion process. The hole boundary is very sharp, and the thickness of sheet metal becomes thinner moving towards the hole (Fig. 6c). The inlet duct of the fan has a 90° configuration determining a sort of elbow in correspondence to the inlet cone. State this condition and the particle mass and diameter, the impacts are localized in the outer side of the cone driven by the particle inertia. The last stationary component is the fan volute. This component collects the contaminated airflow supplied by the impeller. The combination of the flow velocity and the particle inertia determines that the erosion phenomenon affects the rear part and the inner circular surface of the volute the most. Looking at Fig. 6f, the hardfacing plates appear affected by the impact showing visible cracks oriented according to the airflow direction. The majority of the volute surface (see Fig. 6e,h) is affected by a tangential particle impact, while only a small portion (in the proximity of the tongue) experienced higher velocity and lower impact angle. In this region, similar to that found through on-field detections (Fig. 6i), the impact velocity pattern shows the highest values (Fig. 6g), as well as the impact angle, which assumes lower values (Fig. 6h). The elongated shape of the hole demonstrates that the impact process is localized and oriented according to the flow field and, in turn, the particle impact patterns.

The proper representation of the most-affected region by numerical simulation gives a chance to overcome several limitations in the erosion-prediction strategy. First, since the erosion phenomenon combines the particle impact conditions with the substrate resistance, the numerical model allows the calculations of the impact characteristics (velocity and angle), providing the possibility to reproduce it on a test bench where the erosion phenomenon is reproduced and controlled in terms of impact process, dust load and erosion effects (weight loss and microstructural modification of the substrate).

Starting from the impact patterns reported in Figs. 5, 6, the impact velocity and angle statistics were derived. Table 1 collects the ranges of variation on the relevant fan surfaces. Since the fan operates at its design points, several fan regions are characterized by a tangential particle impact (see the blue-colored regions in Figs. 5, 6), while the normal impacts are localized in the separation zone or the regions close to a sudden flow path variations (steps, and elbows). Therefore, the ranges reported in Table 1 cover the overall conditions, albeit some boundary values interested only a small portion of the given region. To complete the erosion assessment, the impact ratio values were also reported. The impact ratio represents the number of particles that impact the surface with respect to the injected particles. From the analysis, the most affected regions are the impeller pressure side and the impeller disk (the volute surfaces have been impacted by the total amount of particles since the volute collected the entire flow rate). Instead of their low amount of impacted particles, the impeller leading edge and the fan shaft have been characterized by the broadest impact angle ranges.

3. Materials and methods

3.1. Microstructural analyses on the hardfacing

To clarify the reasons for the occurred unpredictable erosion damage, the erosive wear behavior of the wear resistance steel Creusabro® 4800 and the Fe-Cr-C hardfacing alloy was experimentally and numerically investigated, starting from their chemical and microstructural features.

Creusabro® 4800 is high-performance wear-resistant steel whose mechanical properties could be improved by alloying elements (i.

Table 1
Impact conditions and ratio of the relevant fan surfaces (ranges).

	Pressure side	Suction side	Leading edge	Impeller disk	Impeller shroud	Inlet cone	Shaft	Volute
Velocity [m/s]	20 – 75	7 – 20	0 – 70	30 – 77	15 – 35	40 – 60	15 – 80	15 – 60
Angle [°]	0 – 10	5 – 22	0 – 50	0 – 30	5 – 15	0 – 30	30 – 90	0 – 30
Impact ratio [%]	18	9	6	34	5	3	5	≈100

e., Cr, Ni, Mo, and Ti) and specific heat treatment procedures. Compared to water-quenched steel with 400 HB of hardness, Creusabro® 4800 has a superior plastic deformation resistance that leads to a delayed detachment of metal particles and, thus, a lower weight loss than conventional steels. However, it is well established that wear resistance is not only related to the hardness, but chemical composition and microstructure play a key role in the actual performance of the material. According to the producer's information, Creusabro® 4800 shows a bainite-martensite mixed microstructure with retained austenite absorbing impact: under the action of local plastic deformations, the surface hardening effect takes place, achieving an increase of hardness of about an additional 70 HB. This phenomenon, called Transformation Induced Plasticity (TRIP) effect, promotes the deformational transformation of residual austenite into martensite and strongly improves the wear resistance.

The Fe-Cr-C hardfacing alloy used in the present investigation to mitigate erosion damage in specific parts of the fan is an HCCI alloy. Such alloy is a Nb- and Mo-rich cast iron whose wear resistance is strongly associated with the microstructure, i.e., size [60], orientation [61], as well as volume fraction [62], and type of carbides.

The chemical composition of the investigated alloys, examined through the Glow Discharge Optical Emission Spectrometry (GD-OES, Spectruma Analitik GDS 650, Hof, Germany) technique, is given in Table 2.

The microstructural investigations were conducted following the standard metallographic procedures, i.e., cutting, mounting in resin, grinding, final polishing, and chemical etching. The latter was performed by Kalling's No. 2 reagent (5 g $CuCl_2$, 100 mL HCl, 100 mL C_2H_5OH): the samples were immersed in the reagent for 5 s, rinsed with ethanol, and air-dried. Metallographic investigations were carried out through a Leica DMi8A (Leica, Wetzlar, Germany) optical microscope (OM) and a Zeiss EVO MA 15 (Zeiss, Oberkochen, Germany) scanning electron microscope (SEM) equipped with an Oxford X-Max 50 (Oxford Instruments, Abingdon-on-Thames, UK) energy dispersive microprobe for semi-quantitative analyses (EDS). The SEM micrographs were recorded in secondary electron (SE-SEM) and back-scattered electron (BSE-SEM) modes. In addition, measurements of Vickers hardness were conducted on the as-polished surfaces of the samples with the VH Metkon (Metkon Instruments Inc., Bursa, Turkey) Vickers hardness tester, in agreement with the ASTM E92 standard, under a 30 kgf test load and 15 s dwelt time (HV30). The mean Vickers hardness was calculated from five indentations.

3.2. Erosive wear tests

The erosive wear tests were conducted through a test rig in accordance with the ASTM G76 standard [34] and constructed on purpose. To study the erosion behavior of the investigated alloys due to a micro-sized powder, the feeding systems, as well as the nozzle, were modified with respect to the prescribed ones to ensure a constant feeding rate and to avoid clogging phenomenon during the test based on the raw mill micro-sized powder. As seen in Fig. 7a, the test rig comprises two main parts: the test section and the particle injection system. The latter is positioned in the upper part of the test bench, composed of a particle feeder and a mixing chamber, while the test section, located at the bottom of the injection system, is composed of a nozzle and a target holder. Fig. 7a shows a digital image of the test section labeled the main components. A detailed description of the adopted test rig can be found in [58].

The erosion tests comprised the analysis of the raw meal powder commonly used in a cement factory, able to form several agglomerates due to humidity and characterized by an average diameter of 4.3 μm ($d_{90} = 9.7$ μm), with a density of 2700 kg m^{-3} (more details in [51,58]). Due to their nature, the agglomeration process is very effective, and the feeding systems were tuned to avoid this phenomenon, ensuring the proper contamination of the airflow closer to the actual conditions. In addition to the particle diameter distribution and overall average density measurements [58], X-ray diffraction (XRD) analyses were performed using the Bragg-Brentano geometry on a Bruker D8 Advance diffractometer equipped with a Cu filament (Kα, 1.5406 Å). All patterns were acquired in the 2θ range of 15° to 75° with 0.02° of step size and 1 s of step time.

Before the erosion tests, both Creusabro® 4800 and HCCI plates were cut (by a water-jet process) to obtain samples with a footprint dimension of 20 mm × 20 mm, whose top surface was ground, polished (mirror-like finishing up to 1 μm diamond paste), and ultrasonically cleaned in acetone. The samples overlook the nozzle at a fixed distance equal to 10 mm according to the standard.

After each erosion test, every sample was cleaned in acetone through an ultrasonic bath to remove any contamination from the erodent powder. The erosion resistance was determined by weighing each specimen before and after the erosion test through a Kern ABT 100-5NM (Kern, Balingen, Germany) analytical balance with an accuracy resolution of 0.01 mg. The erosion resistance, in terms of weight loss, was determined as the average of five tests to check the reproducibility of the phenomenon. As reported in the next paragraph, using such weighting devices matches the necessity of a proper full-scale value (100 g in this case) for measuring a hardfacing sample to reduce the measurement uncertainty. Both conditions imply an adequate selection of the erosion test conditions. Finally, the worn surface of the samples was analyzed by OM, considering the cross-section surface. Hence, they were cut in the center of the erosion crater, according to a cut section through the sample thickness, and prepared following the above-described metallographic technique.

The X-ray diffraction pattern and the SE-SEM image of the used raw meal powder are displayed in Fig. 8a and Fig. 8b, respectively.

Table 2
Chemical composition (wt. %) of the investigated alloys.

	Composition (wt. %) – Fe balance										
	C	Mn	Si	Cr	Mo	Nb	W	V	S	Ni	P
HCCI	3.92	0.62	1.17	20.68	1.94	4.49	0.86	0.53			
Creusabro® 4800	0.22	1.61	0.39	1.59	0.18	–	–	–	0.003	0.14	0.012

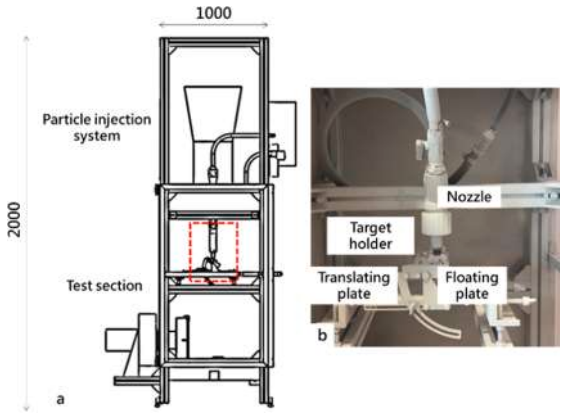

Fig. 7. Images of the erosion test rig: (a) overview of the test rig and (b) detail of nozzle and tiltable table.

As can be seen from the diffraction pattern, the erodent powder is mainly composed of calcite ($CaCO_3$), quartz (SiO_2), and hematite (Fe_2O_3), with traces of alumina (Al_2O_3). As reported in [63], a similar powder sample showed a significant dependency on the impact velocity and was responsible for the fracture of carbides at a normal impact angle (note that this result was obtained for a powder with an order of magnitude greater diameter than the present one). These findings were taken into consideration to select the current test conditions. From the SE-SEM image, the morphology of the erodent particles can be detected: most of them present a round shape and a regular surface morphology.

3.3. Test conditions

To discover the erosion behavior by representative tests, the lab-scaled erosion process was set up looking at the impact analysis, reported in Figs. 5, 6 and summarized in Table 1. Since (i) the erosive powder was obtained directly from the cement plant, and (ii) the assessment of the erosion process was based on the weight differences obtained before and after the tests, the impact conditions were accurately defined to (i) explore the widest test matrix and (ii) reducing the uncertainty of the weight estimations. This means that if the impact velocity value is chosen too low to allow an appreciable weight variation, the exposure time has to be increased, determining a greater powder consumption to complete the test matrix. From these considerations, the erosion tests used a constant powder-feeding rate (10 g min^{-1}) for an exposure time of 30 min, and three different particle impact velocities of 50 m s^{-1}, 100 m s^{-1}, and 150 m s^{-1} were considered. Looking at Table 1, these velocity values cover the majority of the ranges detected by the numerical model, preserving the compromise between the possibility of exploring several impact angles and reducing the measurement uncertainty. State the literature models and data [9], the erosion-velocity correlation is usually provided as a monotonous trend and, due to this, with reference to the three selected values, the extrapolation towards lower and higher velocity values appears adequately feasible. Finally, to set up a test matrix as most comprehensive as possible, five impact angle values as 15°, 30°, 45°, 60°, and 90° were chosen. As reported in the literature [9,64], the angle function assumes a specific trend depending on the substrate characteristics. Therefore, five equally-distributed angle values, from tangential to normal impact conditions, allow a reliable description of this function. A selected impact angle was imposed by tilting the table (see Fig. 7b) and adjusting the distance between the nozzle outlet section and the target surface to ensure a fixed distance of 10 mm. Regarding the temperature of the plate and flow, it was assumed that, since the resistant plates work in a temperature range of (110 – 120) °C that is far from the threshold value indicated by the manufacturer

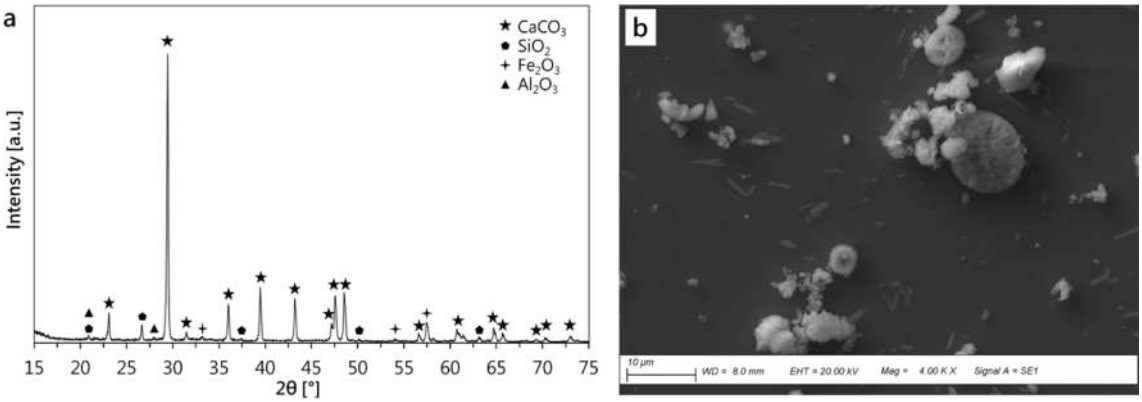

Fig. 8. X-ray diffraction pattern of the erodent powder with phase identification.

datasheet (350 °C – 450 °C), the erosion test were performed at the room temperature. In addition, it has been indicated [9] that the effect of temperature on the erosive resistance is negligible under 200 °C.

4. Results

4.1. As-received material

Fig. 9 shows the results of the microstructural investigations, both with OM and SEM, performed on the Creusabro® 4800 steel. The microstructure of such wear-resistant steel consists of sorbite (Fig. 9a) with areas of slatted martensite (Fig. 9b). The resistance to wear is improved by the fine dispersion of hard micro-alloyed carbides, as the Ti-based one detected by the EDS analysis (Fig. 9c). The bulk hardness results in 736 ± 9 HV30.

Concerning the HCCI, Fig. 10a displays the surface appearance of the as-received plate, and Fig. 10b depicts the microstructural features of the alloy obtained by OM analysis. As can be seen from Fig. 10a, the bead pattern, i.e., juxtaposed passes with continuous overlap, are detectable, as well as the regularly spaced stress relief cracks resulting from the relaxation of heat stress, which develops at right angles to the weld beads. The optical micrograph of the investigated HCCI (Fig. 10b) shows a microstructure composed of pro-eutectic coarse hexagonal M_7C_3 carbides embedded in a matrix of eutectic carbides, austenite, and traces of martensite. The presence of Nb (see Tab. II) enables the precipitation of Nb-rich MC carbides, displayed as polygonal-shaped structures highlighted by red circles in Fig. 10b. In addition, to Nb-rich carbides, from the high magnification, BSE-SEM micrograph of Fig. 11a and the EDS elemental mapping of alloying elements of Fig. 11b, Mo- and Fe-rich carbides were also detected. The bulk hardness results in 714 ± 49 HV30.

4.2. Erosive wear behavior

Fig. 12 reports the erosion test results, in terms of weight loss against impact velocity, for both alloys at a fixed impact angle of 90°. Although the normal impact condition represents the reference point to study erosion behavior, as suggested in the literature models

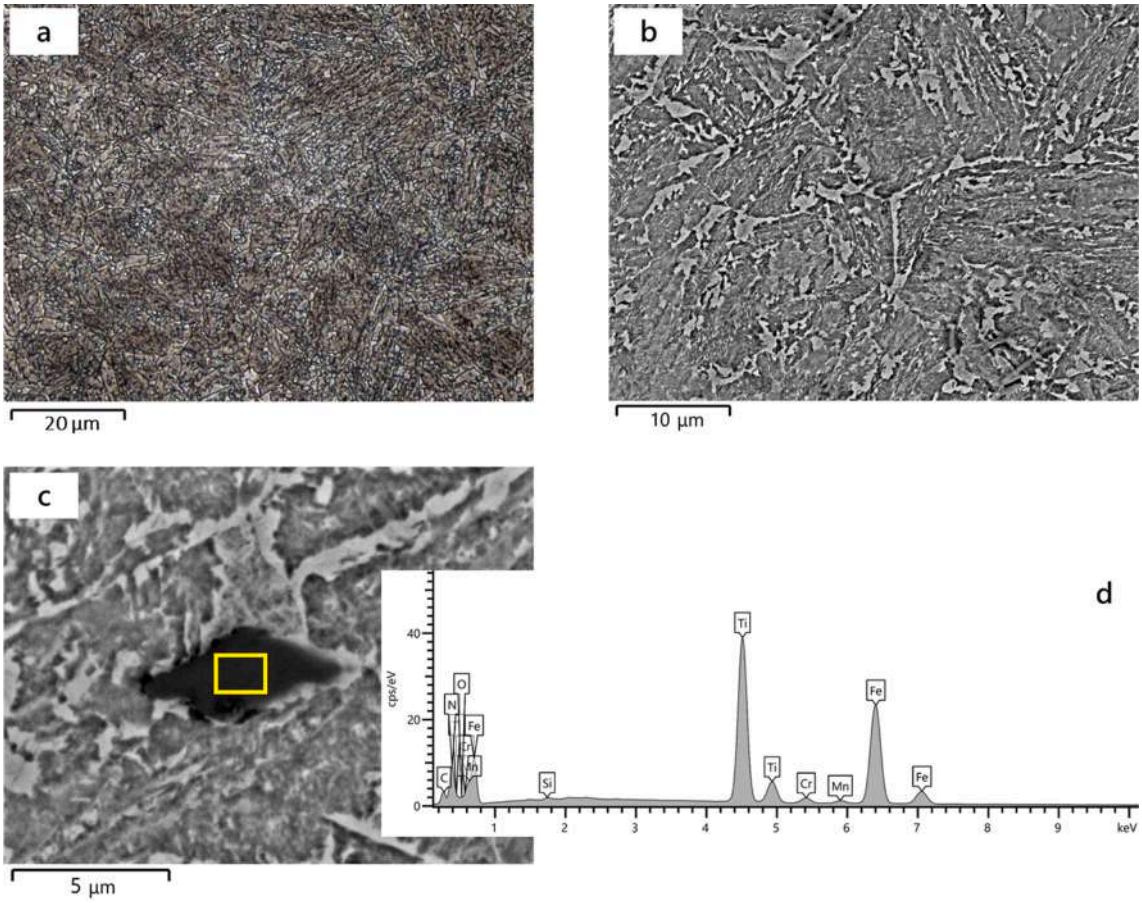

Fig. 9. Metallographic features of the Creusabro® 4800 steel: (a) OM micrograph, (b) BSE-SEM micrograph of the overall microstructure, (c) BSE-SEM micrograph, and (d) EDS spectrum of a Ti carbide.

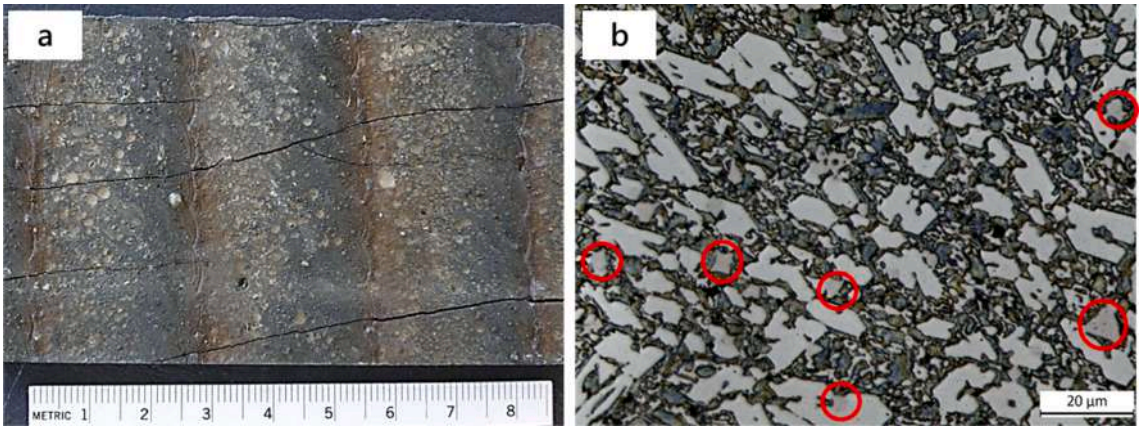

Fig. 10. HCCI characteristics: (a) digital image of the as-received wear-resistant plate, (b) OM micrograph of the overall microstructure, with Nb-rich MC carbides, highlighted by red circles, that appears as polygonal-shaped structures. (For interpretation of the references to colour in this figure legend, the reader is referred to the web version of this article.)

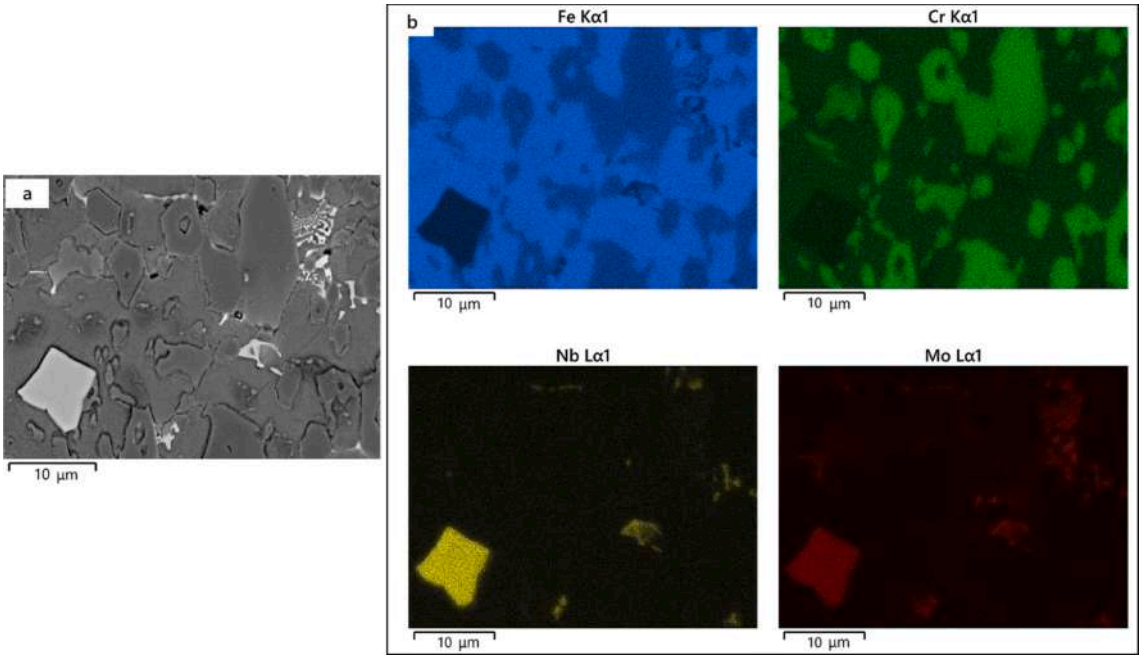

Fig. 11. SEM analyses of the HCCI hardfacing alloy: (a) BSE-SEM micrograph, (b) SEM-EDS elemental mapping.

[22,64], the erosion prediction was made according to the set of coefficients representing the erosion intensity with respect to the effects discovered at 90°. As for the wear-resistant steel, the weight loss increases as the impact velocity increases, from 50 m s^{-1} to 150 m s^{-1}. Conversely, for the HCCI, the weight loss increases with the impact velocity up to 100 m s^{-1} and then slightly decreases for the highest tested impact velocity. At the highest impact velocity, the weight loss of the HCCI is about three times lower than the wear-resistant steel.

As for the role of the impact angle, Fig. 13 reports the erosion test results for the investigated HCCI (Fig. 13a) and wear-resistant steel (Fig. 13b). As seen, for the HCCI, regardless of the impact velocity, the weight loss data show a weak dependence on impact angle. Conversely, maximum erosion occurs at shallow impact angles for wear-resistant steel, and this trend is comparable for all the considered impact velocities.

In Figs. 12, 13, the estimation of the variability of the results was reported by error bars. The magnitude of the bars was obtained by the procedure reported in [52,65] based on at least five runs for each tested condition. State the data dispersion due to the substrate characteristics, the uncertainty of the weighting process, estimated in ± 0.06 mg [33,58], is comprised in the previous assessment.

For a better understanding of this statement and to further describe the erosion behavior of these materials, the metallographic analysis of the cross-section of the erosion crater was taken into account. Fig. 14 reports the optical micrographs of the cross-sections at

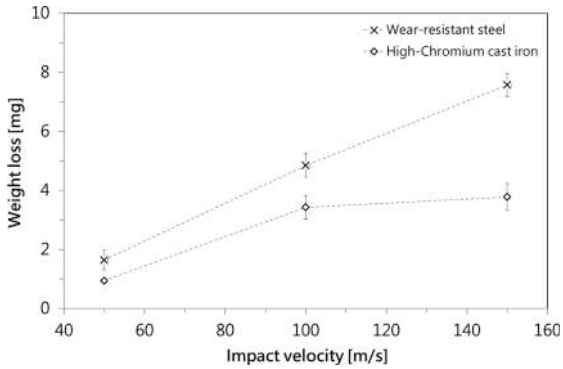

Fig. 12. Erosion tests results: weight loss for wear-resistant steel and high-Chromium cast iron against impact velocity for an impact angle of 90°.

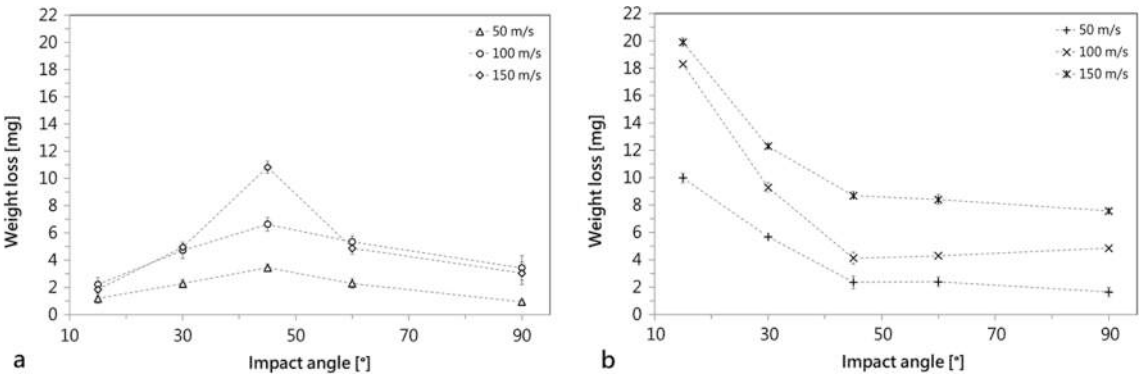

Fig. 13. Erosion tests results: weight loss against impact angle for (a) HCCI and (b) wear-resistant steel.

the center of the craters for the wear-resistant steel (Fig. 14a) and the HCCI (Fig. 14b), respectively. These micrographs are pertaining to the wear tests performed at an impact velocity of 100 m s^{-1} for an impact angle of 90°, and the contaminated airflow is supplied from the top to the bottom of the reported images. In Fig. 14a, the wear-resistant steel is characterized by uniform thickness reduction over the investigated region. By contrast, in Fig. 14b, the HCCI shows an irregular profile, very similar to a grooved path: the erosion process has developed differently in the matrix and the carbides.

5. Discussion

With reference to the microstructure of HCCIs, and, more in detail, to the morphology of the Cr-rich carbides, the formation and growth of such rod-like shape primary carbides depend on the direction of the heat flow, as suggested by their morphology. As seen in Fig. 10b, they display an irregular polygonal shape with several hollows in the center and gaps on the edge, according to the growth characteristics process proposed in the literature [66].

The erosive wear behavior of the wear-resistant steel and the HCCI was experimentally tested by evaluating the impact velocity and angle effect. The weight loss against impact velocity graph enables the direct comparison between wear-resistant steel and high-chromium cast iron. The reported trend for wear-resistant steel is consistent with the pioneering work of Finnie [22], which suggested a direct proportionality between the erosion damage and particle impact velocity, more specifically, the kinetic energy of the incoming particle. It can also be observed the higher erosion resistance of the HCCI in comparison with the wear-resistant steel: as reported in the literature [67], HCCI displays higher abrasion resistance than mild steel when the abrasive particles are softer than the carbide particles. In this respect, as pointed out by Sapate and RamaRao [67], the cement clinker (412 ± 123 HV0.1) is softer than the observed Cr-based and Nb-based carbides for which hardness values higher than 1,500 HV0.1 were found. Besides, the data in Fig. 12 also suggest the advantages related to the use of hardfacing alloys in relation to the life prediction of the fan. Looking at the material loss values for the two materials (each test is characterized by the same contaminant concentration and exposure time), the HCCI shows lower values. At low-impact velocity, the material loss is half that of wear-resistant steel. This difference increases moving towards the highest velocity, at which the material loss is three times the HCCI value. In a simplified line of thought, assuming a linear erosion process over time, which means a constant contaminant concentration and avoiding the geometry modification of the substrate (i.e., the impact conditions driven by the flow field do not change), the useful operating life of a fan equipped with HCCI is double (or triple) than a fan built with common wear-resistance steel.

The HCCI plates require more significant manufacturing costs related to the plates and their installations on the relevant fan

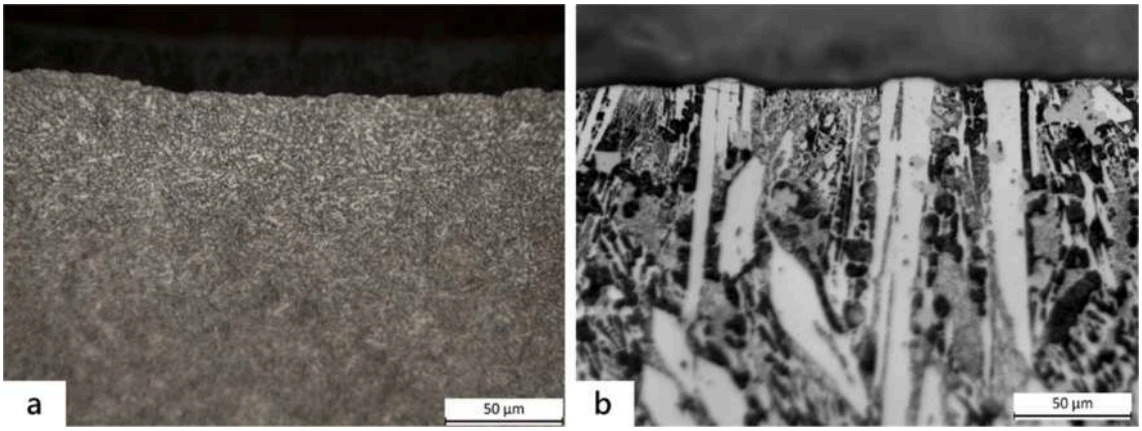

Fig. 14. OM micrographs of the worn cross-section of the craters: (a) wear-resistant steel, (b) HCCI.

surface. The installation involves the welding process and tailored cuts to match the fan surfaces preserving the aerodynamic design of the unit. This downside has to be included in the overall evaluation of the erosion resistance to match the technical and economic points of view.

In addition, the effect of the impact velocity on weight loss was also considered. It is widely accepted [17,32] that the erosion of ductile materials (e.g., most of the metals) strongly depends on impact angle showing the maximum erosion at shallow impact angles (around 20° – 30°) and reduced erosion at normal impact angle since the particles tend to be embedded and no removal of material occurs. Conversely, brittle metals break easily at a normal impact angle and show maximum wear damage. The observed behavior of the HCCI, i.e., regardless of the impact velocity, the weight loss data show a weak dependence on impact angle, has also been observed by Sapate and RamaRao [67], despite in all cases, the highest weight loss is at 45° of impact angle. As recently claimed by Tarodiya and Levy [9], the erosive wear behavior of HCCI is still under investigation since ductile, brittle, and weak dependence on impact angles has been found.

Regarding wear-resistant steel, the maximum erosion observed at shallow impact angles has also been reported in the literature for ductile materials. Such behavior is in accordance with the microstructural observations of the worn cross-section of the craters. As seen, the primary M_7C_3 carbides emerge from the surface as a result of the damage by the erodent particles. These findings may indicate that harder and uniformly distributed carbides guarantee an increased wear resistance since the erodent particles cannot get into the matrix, and carbides are not easily separated from it. Considering the hardness of the carbides and the matrix, it is reasonable to suppose that the erosion of the matrix gives a ductile-type erosion while the carbide erosion is more similar to a brittle-type phenomenon, as reported by the trends in Fig. 13 and as suggested in literature [63].

5.1. *Summary and suggestions*

The wear issue related to solid particle erosion is crucial for heavy-duty centrifugal fans operating in cement or steel production plants or as a part of exhaust systems in mines or energy production plants. The stationary and rotating components of these machines are affected by severe erosion phenomena over their operative life due to the high-velocity flow (over 100 m s^{-1}) and the relevant solid contaminant concentration.

In this framework, this work has been developed for improving the comprehension of such a complex phenomenon as SPE by numerical and experimental tools, from which some specific issues should be addressed:

- Effectiveness of an experimental–numerical approach: adopting a combined strategy enables a better comprehension of the erosion behavior that affects the fan, increasing the prediction capability of both the design solutions and the overhaul operations. Indeed, the proper selection of the hardfacing alloy and its location through the fan flow path are the results of a numerical-experimental coupled strategy. In this way, the erosion issues could be prevented and/or limited without affecting too much the machine manufacturing/overhaul costs;
- Optimized design: the results of the experimental investigation have highlighted a non-trivial conclusion in relation to the estimation of the erosion-resistant properties of the tested substrate. The hardness of the substrate is not sufficient to comprehend the evolution of erosion. The erosion test campaign demonstrates how the impact process determines a non-linear phenomenon according to the impact angle and material properties. In light of these results, only by considering the contaminant trajectories is it possible to exploit the best compromise between operating life and costs. The HCCI plates require higher material and installation costs, and their usage has to be carefully checked to exploit the best erosion-resistant results with the minimum cost. It can also be remarked that the critical point of these installations is not the elimination of the erosion issue (that is not feasible considering the operating condition and the resistance of HCCI) but the capability to make a reliable prediction of the working life of the unit. Assuming this concept as a guideline for the design of the unit, the installation of the wear-resistant plate goes hand in hand with

the analysis of the erosion phenomenon coupled with the estimation of the contaminant path through the unit (an example of this is the installation of erosion shield for bolts that represent a sort of sacrificial material to protect the bolts form erosion during the operating life);

- Predictive maintenance: monitoring the critical areas has to be carried out periodically to check the status of the components, even if the best wear protection has been adopted. Systematic vibration monitoring, regular visual inspection of the impellers, and monitoring of the bearing temperature are highly recommended. Finally, even though the chemical composition of hardfacing alloys is compatible with high demanding wear environments, worn areas could be re-hardfaced. In a nutshell, early detection of wear in centrifugal fans and the corresponding repair measures are very cost-effective;
- Preventive maintenance: erosion contributes to the reduction of reliability and safety of the whole plant and leads to a decrease in the machine's efficiency. More specifically, if maintenance operations are postponed or even ignored, premature failures of the components, with potentially severe consequences for human safety, may occur. On the other hand, the proper scheduling of maintenance intervals along with the operative life of the machine is not possible without a deep understanding of the mechanisms involved in the particle erosion phenomenon. Scheduling overhaul operations is challenging due to the significant number of unknowns involved in the life cycle analysis of such machines. As a result, inspection operations are often regularly scheduled, leading to the shutdown of the production plant with high costs in terms of man-hours and plant downtime. Hence, developing a methodology to estimate the erosion severity and assess the time to overhaul, based on experimental data obtained in controlled conditions, may aid the sales and maintenance engineers in a proper schedule of such operations. Regarding this issue, in [52], a simple relation relating the time to overhaul to the main erosion and fan working and design parameters is proposed;
- Failure analysis on a custom device: the numerical analysis shows that for a centrifugal fan exposed to a contaminated airflow, each relevant surface (of stationary or rotating part) experiences a different impact process according to the impact velocity and angle. These conditions determine different erosion behavior, which is responsible for the contemporary presence of highly-eroded regions and regions which have preserved their former integrity. To overcome this understanding lacks, the numerical results (in terms of impact) act as the starting point of the experimental campaign, primarily if the tests are based on the actual substrate and contaminants materials and/or the failure analysis is on a custom device for which the overall operative conditions could not be otherwise reproduced on a standard test bench.

6. Conclusions

The present paper focuses on studying the root causes of the failure of a fan operating in a cement factory. The operating production plant was investigated through a combined approach consisting of specific experimental wear tests and numerical analyses. Even if it is known that deciphering the failure of machinery components through understanding the root cause is a complex and challenging task, such a combined approach proved to be quite effective.

The experimental campaign focused on the effects of impact velocity and impact angle of the erodent particles on the erosive mass loss of the substrate, enabling to assess and compare the erosive wear behavior of both the wear-resistant steel and the HCCI. It was found that Creusabro ® 4800 steel is characterized by lower wear resistance to abrasive wear for all the investigated impact velocities. Conversely, the HCCI shows superior wear resistance, as confirmed by the microstructural investigations. Indeed, the alloying elements of the HCCI promote the formation of hard carbides that can better withstand the severe erosive conditions experienced by the fan and simulated by the erosive wear tests.

Fluid dynamic simulations enabled to obtaining of a first attempt estimation of the wear pattern on the machine and allowed the calculation of the actual impact behavior, which has been used to define the most representative test matrix, i.e., reproducing the actual impact behavior on and erosion process. Therefore, the cross-correlation between the particle impact behavior coming from the virtual analysis, the erosion effects discovered using the experimental test bench, and the on-field damage detections have been set up.

Based on the reported results, it can be concluded that the most likely cause of the failure is closely related to the material selection regarding the operating environment. Given the severe erosive conditions in which the fan is working, the adoption of HCCI hardfacing plates, instead of the classical wear-resistant steel, is proven to be effective in increasing the lifetime of the critical parts.

The overall results contribute to a better understanding of the microstructure–property relationships concerning the erosive wear resistance of classical wear-resistant steel and high chromium cast iron. As a result, it is possible to prevent premature damage to the components by the proper selection of the critical metallurgical features of the materials. Besides, the engineering failure analysis combined with detailed research analyses reduces the incidences of failures and extends the operating horizons of engineering materials.

Declaration of Competing Interest

The authors declare that they have no known competing financial interests or personal relationships that could have appeared to influence the work reported in this paper.

Data availability

No data was used for the research described in the article.

Acknowledgments

The authors express special thanks to Eng. Paolo Saccenti of Boldrocchi S.r.l. (Biassono, Monza-Brianza, Italy) for his support during the research activities. Thanks to Prof. Michele Pinelli and Prof. Mattia Merlin for the coordination and support. A special thanks go to Eng. Mattia Alemanni for his contribution concerning the Creusabro® 4800 wear-resistant steel.

References

[1] K.G. Budinski, S.T. Budinski, Tribomaterials: Properties and Selection for Friction, Wear, and Erosion Applications, ASM International, 2021. https://doi.org/10.31399/asm.tb.tpsfwea.9781627083232.
[2] I. Kleis, P. Kulu, Solid Particle Erosion, Springer, London, London (2008), https://doi.org/10.1007/978-1-84800-029-2.
[3] S.C. Lim, A.W. Batchelor, C.Y.H. Lim, Introduction and Basic Theory of Wear, in: G.E. Totten (Ed.), Frict. Lubr. Wear Technol., ASM International, 2017: pp. 223–224. https://doi.org/10.31399/asm.hb.v18.a0006357.
[4] İ. Özen, H. Gedikli, B. Öztürk, Improvement of solid particle erosion resistance of helicopter rotor blade with hybrid composite shield, Eng. Fail. Anal. 121 (2021), 105175, https://doi.org/10.1016/j.engfailanal.2020.105175.
[5] L. Cao, S. Liu, P. Hu, H. Si, The influence of governing valve opening on the erosion characteristics of solid particle in steam turbine, Eng. Fail. Anal. (2020), https://doi.org/10.1016/j.engfailanal.2020.104929.
[6] A. Evstifeev, N. Kazarinov, Y. Petrov, L. Witek, A. Bednarz, Experimental and theoretical analysis of solid particle erosion of a steel compressor blade based on incubation time concept, Eng. Fail. Anal. 87 (2018) 15–21, https://doi.org/10.1016/j.engfailanal.2018.01.006.
[7] B. Liu, J. Zhao, J. Qian, Numerical analysis of cavitation erosion and particle erosion in butterfly valve, Eng. Fail. Anal. 80 (2017) 312–324, https://doi.org/10.1016/j.engfailanal.2017.06.045.
[8] A. Suman, N. Casari, E. Fabbri, L. di Mare, F. Montomoli, M. Pinelli, Generalization of particle impact behavior in gas turbine via non-dimensional grouping, Prog. Energy Combust. Sci. 74 (2019) 103–151, https://doi.org/10.1016/j.pecs.2019.05.001.
[9] R. Tarodiya, A. Levy, Surface erosion due to particle-surface interactions - A review, Powder Technol. 387 (2021) 527–559, https://doi.org/10.1016/j.powtec.2021.04.055.
[10] G.R. Desale, B.K. Gandhi, S.C. Jain, Particle size effects on the slurry erosion of aluminium alloy (AA 6063), Wear. 266 (2009) 1066–1071, https://doi.org/10.1016/j.wear.2009.01.002.
[11] A. Abouel-Kasem, Particle Size Effects on Slurry Erosion of 5117 steels, J. Tribol. 133 (2011), https://doi.org/10.1115/1.4002605.
[12] A.V. Levy, P. Chik, The effects of erodent composition and shape on the erosion of steel, Wear. 89 (1983) 151–162, https://doi.org/10.1016/0043-1648(83)90240-5.
[13] H. Arabnejad, S.A. Shirazi, B.S. McLaury, H.J. Subramani, L.D. Rhyne, The effect of erodent particle hardness on the erosion of stainless steel, Wear. 332–333 (2015) 1098–1103, https://doi.org/10.1016/j.wear.2015.01.017.
[14] Z. Feng, A. Ball, The erosion of four materials using seven erodents — towards an understanding, Wear. 233–235 (1999) 674–684, https://doi.org/10.1016/S0043-1648(99)00176-3.
[15] B.A. Lindsley, A.R. Marder, The effect of velocity on the solid particle erosion rate of alloys, Wear. 225–229 (1999) 510–516, https://doi.org/10.1016/S0043-1648(99)00085-X.
[16] M.A. Islam, Z.N. Farhat, Effect of impact angle and velocity on erosion of API X42 pipeline steel under high abrasive feed rate, Wear. 311 (2014) 180–190, https://doi.org/10.1016/j.wear.2014.01.005.
[17] G.R. Desale, B.K. Gandhi, S.C. Jain, Effect of erodent properties on erosion wear of ductile type materials, Wear. 261 (2006) 914–921, https://doi.org/10.1016/j.wear.2006.01.035.
[18] G.R. Desale, B.K. Gandhi, S.C. Jain, Slurry erosion of ductile materials under normal impact condition, Wear. 264 (2008) 322–330, https://doi.org/10.1016/j.wear.2007.03.022.
[19] E. Hornbogen, The role of fracture toughness in the wear of metals, Wear. 33 (1975) 251–259, https://doi.org/10.1016/0043-1648(75)90280-X.
[20] D.G. Bhosale, T.R. Prabhu, W.S. Rathod, M.A. Patil, S.W. Rukhande, High temperature solid particle erosion behaviour of SS 316L and thermal sprayed WC-Cr3C2–Ni coatings, Wear. 462–463 (2020), 203520, https://doi.org/10.1016/j.wear.2020.203520.
[21] A. Levy, Y.-F. Man, Surface degradation of ductile metals in elevated temperature gas-particle streams, Wear. 111 (1986) 173–186, https://doi.org/10.1016/0043-1648(86)90218-8.
[22] I. Finnie, Erosion of surfaces by solid particles, Wear. 3 (1960) 87–103, https://doi.org/10.1016/0043-1648(60)90055-7.
[23] M. Parsi, K. Najmi, F. Najafifard, S. Hassani, B.S. McLaury, S.A. Shirazi, A comprehensive review of solid particle erosion modeling for oil and gas wells and pipelines applications, J. Nat. Gas Sci. Eng. (2014), https://doi.org/10.1016/j.jngse.2014.10.001.
[24] B.G. Mellor, Surface coatings for protection against wear (2006), https://doi.org/10.1533/9781845691561.
[25] J. Hornung, A. Zikin, K. Pichelbauer, M. Kalin, M. Kirchgaßner, Influence of cooling speed on the microstructure and wear behaviour of hypereutectic Fe–Cr–C hardfacings, Mater. Sci. Eng. A. 576 (2013) 243–251, https://doi.org/10.1016/j.msea.2013.04.029.
[26] A.A. Pauzi, M.J. Ghazali, W.F.H.W. Zamri, A. Rajabi, Wear Characteristics of Superalloy and Hardface Coatings in Gas Turbine Applications–A Review, Metals (Basel). 10 (2020) 1171, https://doi.org/10.3390/met10091171.
[27] L.-E. Svensson, B. Gretoft, B. Ulander, H.K.D.H. Bhadeshia, Fe-Cr-C hardfacing alloys for high-temperature applications, J. Mater. Sci. 21 (1986) 1015–1019, https://doi.org/10.1007/BF01117388.
[28] S.M. Yunus, A.A. Pauzi, S. Husin, Wear Prediction via Accelerated Test on Chromium Based Hard Coatings for Gas Turbine Interfaces Applications Up to 370 °C, IOP Conf. Ser. Mater. Sci. Eng. 429 (2018), 012063, https://doi.org/10.1088/1757-899X/429/1/012063.
[29] V.K. Afanasyev, A.P. Chernysh, S.V. Dolgova, Restoration of agricultural machines surfaces by white cast iron with the formation of technological repair units, Mater. Sci. Forum. (2018), https://doi.org/10.4028/www.scientific.net/MSF.927.43.
[30] ASTM A532. Standard Specification for Abrasion-Resistant Cast Irons, (2019). https://doi.org/10.1520/A0532_A0532M-10R19.
[31] G. Straffelini, Friction and Wear, Springer International Publishing, Cham (2015), https://doi.org/10.1007/978-3-319-05894-8.
[32] I. Hutchings, P. Shipway, Tribology: Friction and wear of engineering materials: Second Edition, Elsevier Inc., 2017.
[33] A. Fortini, A. Suman, N. Zanini, G. Cruciani, Erosive Wear Behavior of High-Chromium Cast Iron: Combined Effect of Erodent Powders and Destabilization Heat Treatments, Coatings. 12 (2022) 1218, https://doi.org/10.3390/coatings12081218.
[34] ASTM G76: Standard Test Method for Conducting Erosion Tests by Solid Particle Impingement Using Gas Jets, (2012). https://doi.org/10.1520/G0076-18.
[35] J.J. Coronado, H.F. Caicedo, A.L. Gómez, The effects of welding processes on abrasive wear resistance for hardfacing deposits, Tribol. Int. (2009), https://doi.org/10.1016/j.triboint.2008.10.012.
[36] M.F. Buchely, J.C. Gutierrez, L.M. León, A. Toro, The effect of microstructure on abrasive wear of hardfacing alloys, Wear. 259 (2005) 52–61, https://doi.org/10.1016/j.wear.2005.03.002.
[37] S. Chatterjee, T.K. Pal, Wear behaviour of hardfacing deposits on cast iron, Wear. 255 (2003) 417–425, https://doi.org/10.1016/S0043-1648(03)00101-7.
[38] A. Gualco, H.G. Svoboda, E.S. Surian, Study of abrasive wear resistance of Fe-based nanostructured hardfacing, Wear. 360–361 (2016) 14–20, https://doi.org/10.1016/j.wear.2016.04.011.
[39] C.M. Chang, Y.C. Chen, W. Wu, Microstructural and abrasive characteristics of high carbon Fe-Cr-C hardfacing alloy, Tribol. Int. (2010), https://doi.org/10.1016/j.triboint.2009.12.045.

[40] P. Li, Y. Yang, D. Shen, M. Gong, C. Tian, W. Tong, Mechanical behavior and microstructure of hypereutectic high chromium cast iron: the combined effects of tungsten, manganese and molybdenum additions, J. Mater. Res. Technol. 9 (2020) 5735–5748, https://doi.org/10.1016/j.jmrt.2020.03.098.
[41] A.N. Stevenson, I. Hutchings, Wear of hardfacing white cast irons by solid particle erosion, Wear. 186–187 (1995) 150–158, https://doi.org/10.1016/0043-1648(95)07184-9.
[42] M. Gucwa, R. Bęczkowski, T. Wyleciał, The effect of the hardfacing sequence on the structure and erosion resistance of high chromium alloy, in: Met. 2017 - 26th Int. Conf. Metall. Mater. Conf. Proc., 2017.
[43] S.G. Sapate, A.V. Rama Rao, Effect of material hardness on erosive wear behavior of some weld-deposited alloys, Mater. Manuf. Process. 17 (2002) 187–198, https://doi.org/10.1081/AMP-120003529.
[44] T.A. Adler, Ö.N. Doğan, Erosive wear and impact damage of high-chromium white cast irons, Wear. 225–229 (1999) 174–180, https://doi.org/10.1016/S0043-1648(99)00010-1.
[45] P.A. Alsop, The cement plant operations handbook, 6th ed.,, Tradeship Publications Ltd, 2019.
[46] A.D. Glasser, W.J. Petlevich, E.F. Sverdrup, Nature and costs of fan erosion on coal-fired electric power plants., (1980).
[47] G.W. McKervey, B. Perry, Fan applications in the cement industry, in: [1993] Rec. Conf. Pap. 35th IEEE Cem. Ind. Tech., IEEE, 1993: pp. 467–476. https://doi.org/10.1109/CITCON.1993.296970.
[48] A.D. Glasser, W.J. Petlevich, E.F. Sverdrup, Nature and costs of fan erosion on coal-fired electric power plants., 1980.
[49] R.P. Mandi, U.R. Yaragatti, Energy efficiency improvement of auxiliary power equipment in thermal power plant through operational optimization, in: 2012 IEEE Int. Conf. Power Electron. Drives Energy Syst., IEEE, 2012: pp. 1–8. https://doi.org/10.1109/PEDES.2012.6484459.
[50] N. Aldi, N. Casari, M. Pinelli, A. Suman, A. Vulpio, P. Saccenti, R. Beretta, A. Fortini, M. Merlin, Erosion behavior on a large-sized centrifugal fan, in: 13th Eur. Turbomach. Conf. Turbomach. Fluid Dyn. Thermodyn. ETC 2019, 2019. https://doi.org/10.29008/ETC2019-389.
[51] N. Aldi, N. Casari, M. Pinelli, A. Suman, A. Vulpio, P. Saccenti, Performance Modification of an Erosion-Damaged Large-Sized Centrifugal Fan, in: Vol. 1 Aircr. Engine; Fans Blowers; Mar. Wind Energy; Sch. Lect., American Society of Mechanical Engineers, 2021. https://doi.org/10.1115/GT2021-59832.
[52] A. Vulpio, S. Oliani, A. Suman, N. Zanini, P. Saccenti, A Mechanistic Model for the Predictive Maintenance of Heavy-Duty Centrifugal Fans Operating With Dust-Laden Flows, J. Eng. Gas Turbines Power. 145 (2023), https://doi.org/10.1115/1.4055709.
[53] G.I. Ilieva, Erosion failure mechanisms in turbine stage with twisted rotor blade, Eng. Fail. Anal. 70 (2016) 90–104, https://doi.org/10.1016/j.engfailanal.2016.07.008.
[54] İ. Özen, H. Gedikli, Solid Particle Erosion on Shield Surface of a Helicopter Rotor Blade Using Computational Fluid Dynamics, J. Aerosp. Eng. (2019), https://doi.org/10.1061/(asce)as.1943-5525.0000962.
[55] M. Mengütürk, E. Sverdrup, Computer Calculation of Fan Erosion in Coal-Fired Power Plants. Part 1: Centrifugal Fans, Int. J. Turbo Jet Engines. 2 (1985) 169–176, https://doi.org/10.1515/TJJ.1985.2.2.169.
[56] L. Cardillo, A. Corsini, G. Delibra, F. Rispoli, A.G. Sheard, P. Venturini, Simulation of Particle-Laden Flows in a Large Centrifugal Fan for Erosion Prediction, in: Vol. 1A Aircr. Engine; Fans Blowers, ASME, 2014: p. V01AT10A014. https://doi.org/10.1115/GT2014-25865.
[57] M. Fritsche, P. Epple, M. Steber, H.J. Rußwurm, Erosion Optimized Radial Fan Impellers and Volutes for Particle Flows, in: Vol. 7 Fluids Eng., American Society of Mechanical Engineers, 2017. https://doi.org/10.1115/IMECE2017-71825.
[58] A. Fortini, A. Suman, A. Vulpio, M. Merlin, M. Pinelli, Microstructural and erosive wear characteristics of a high chromium cast iron, Coatings. (2021), https://doi.org/10.3390/coatings11050490.
[59] A.D. Gosman, E. Ioannides, Aspects of Computer Simulation of Liquid-Fueled Combustors, J. Energy. 7 (1983) 482–490, https://doi.org/10.2514/3.62687.
[60] R. Chotěborský, P. Hrabě, M. Müller, R. Válek, J. Savková, M. Jirka, Effect of carbide size in hardfacing on abrasive wear, Res. Agric. Eng. 55 (2009) 149–158, https://doi.org/10.17221/1/2009-RAE.
[61] Ö.N. Doğan, J.A. Hawk, Effect of carbide orientation on abrasion of high Cr white cast iron, Wear. 189 (1995) 136–142, https://doi.org/10.1016/0043-1648(95)06682-9.
[62] S.G. Sapate, A.V. Rama Rao, Effect of carbide volume fraction on erosive wear behaviour of hardfacing cast irons, Wear. 256 (2004) 774–786, https://doi.org/10.1016/S0043-1648(03)00527-1.
[63] S.G. Sapate, A.V. RamaRao, Effect of Erodent Particle Hardness on Velocity Exponent in Erosion of Steels and Cast Irons, Mater. Manuf. Process. (2003), https://doi.org/10.1081/AMP-120024975.
[64] Y.I. Oka, K. Okamura, T. Yoshida, Practical estimation of erosion damage caused by solid particle impact, Wear. 259 (2005) 95–101, https://doi.org/10.1016/j.wear.2005.01.039.
[65] M. Schrade, S. Staudacher, M. Voigt, M., Experimental and numerical investigation of erosive change of shape for high-pressure compressors, in Vol. 1: Aircraft Engine; Fans and Blowers; Marine, ASME, 2015: p: V001T01A001. https://doi.org/10.1115/GT2015-42061.
[66] S. Liu, Y. Zhou, X. Xing, J. Wang, X. Ren, Q. Yang, Growth characteristics of primary M7C3 carbide in hypereutectic Fe-Cr-C alloy, Sci. Rep. 6 (2016) 32941, https://doi.org/10.1038/srep32941.
[67] S.G. Sapate, A.V. RamaRao, Erosive wear behaviour of weld hardfacing high chromium cast irons: effect of erodent particles, Tribol. Int. 39 (2006) 206–212, https://doi.org/10.1016/j.triboint.2004.10.013.